PAPER

High-throughput *ab initio* screening of binary solid solutions in olivine phosphates for Li-ion battery cathodes

Modelling Simul. Mater. Sci. Eng. **21** (2013) 074004 (16pp) doi:10.1088/0965-0393/21/7/074004

High-throughput *ab initio* screening of binary solid solutions in olivine phosphates for Li-ion battery cathodes

H R Hajiyani, U Preiss, R Drautz and T Hammerschmidt

Interdisciplinary Centre for Advanced Materials Simulation, Ruhr-Universität Bochum, Universitätsstr. 150, 44780 Bochum, Germany

E-mail: hamidreza.hajiyani@rub.de

Received 2 January 2013, in final form 22 July 2013
Published 8 October 2013
Online at stacks.iop.org/MSMSE/21/074004

Abstract

A promising approach to improving the performance of iron-phosphate $FePO_4$ cathode materials for Li-ion batteries is to partly or fully substitute Fe with other metals. Here, we use high-throughput density-functional theory (DFT) calculations to investigate binary mixtures of metal atoms M and M' in $(Li)M_yM'_{1-y}PO_4$ olivine phosphates. We determine the formation energy for various stoichiometries of different binary combinations of metals for the cases of full lithiation and delithiation. Systematic screening of all combinations of Fe and Mn with elements of the 3d transition-metal (TM) series allows us to identify trends with average band filling and atomic size. We also included compounds that verify the observed relations or that were discussed as cathode materials, particularly Ni–Co, V–Cu and V–Ni, as well as combinations with 4d TMs (Fe–Zr, Fe–Mo, Fe–Ag) and with Mg (Fe–Mg and Ni–Mg). Based on our DFT calculations for each compound, we estimate the volume change during intercalation, the intercalation voltage, the energy density and the thermal stability with respect to reaction with oxygen. Our calculations indicate that the energy density of the binary TM phosphates increases with average band filling while the thermal stability of the compounds decreases.

(Some figures may appear in colour only in the online journal)

1. Introduction

One of the central challenges in increasing the performance of Li-ion batteries is the optimization of cathode materials. The possible candidates need to provide a technologically acceptable compromise between energy density, intercalation voltage, capacity and conductivity, as well as structural and thermal stability during operation. A number of compound types is discussed as cathode materials, see, e.g., [1–3] for recent reviews.

In addition to the layered structures (e.g. $LiCoO_2$) and spinel structures (e.g. $LiMn_2O_4$), polyanion-type structures like olivine phosphates are technologically very promising. The most prominent example, $FePO_4$, is particularly suited for battery applications, but also olivine phosphates based on other transition-metal (TM) elements such as Mn, Co and Ni are promising candidates. Since the first synthesis of $FePO_4$ [4], this cathode material with a miscibility gap at room temperature [5] is used commercially in a wide range of Li-ion batteries. However, despite the efforts in optimizing its synthesis (see, e.g., [6–9]), the performance of TM olivine phosphates still suffers from low conductivity due to low-dimensional diffusion (e.g. $FePO_4$), lattice distortions (e.g. $MnPO_4$), comparably low capacities (e.g. $CoPO_4$) or undesirably high operating voltages (e.g. $NiPO_4$). The limited conductivity causes slow battery charging and discharging, a problem that can be partially overcome by carbon coating [10, 11], nanosizing [12] or doping [13].

One of the routes to improve the performance is to substitute Li in the M1 site of olivine phosphate with other metal atoms M as demonstrated, e.g., for M = Mg, Al, Ti, Zr, Nb and W in the case of iron and nickel olivine phosphates [14–16]. Other substitution concepts include doping the phosphorus site, e.g. by vanadium [17]. The M2 site is also accessible to doping or substitution by other TMs at a fixed stoichiometry and over a wide range of chemical compositions in order to optimize the Li-ion mobility, redox potential and cyclability. The investigated systems include Li–(Sc/Fe)PO_4 [13], Li–(Ti/Fe)PO_4 [13, 18], Li–(Zr/Fe)PO_4 [18], Li–(V/Fe)PO_4 [13, 19, 20], Li–(Mn/Fe)PO_4 [21–27], Li–(Fe/Ni)PO_4 [28], Li–(Co/Ni)PO_4 [29], Li–(Mn/Co)PO_4 [30], Li–(Mn/Ni)PO_4 [26], Li–(Mn/Mg)PO_4 [26], Li–(Mn/Zn)PO_4 [26], Li–(Fe/Cu)PO_4 [31], Li–(Fe/Zn)PO_4 [32], Li–(Mo/Fe)PO_4 [33], Li–(Mg/Fe)PO_4 [18], Li–(Mn/Fe/Co)PO_4 [21, 34–36], Li–(Mn/Fe/Mg)PO_4 [37], Li–(Mn/Co/Ni)PO_4 [30] and Li–(Mn/Fe/Co/Ni)PO_4 [38, 39]. The established approaches to increase the conductivity of $FePO_4$ such as carbon coating can also be applied to such multi-component solid-solution compounds [40] with even improved performance [41].

Here, we carry out a systematic screening of substituting Fe in the M2 site in olivine phosphates with other metal atoms. In particular, we perform high-throughput density-functional theory (DFT) calculations in order to determine the formation energy of the solid-solution compounds (Li)$M_yM'_{1-y}PO_4$ at different stoichiometries (y = 0.0, 0.25, 0.50, 0.75, 1.00) of the TMs M and M'. For each combination $M_yM'_{1-y}$ we consider the fully lithiated $LiM_yM'_{1-y}PO_4$ and the fully delithiated $M_yM'_{1-y}PO_4$. Based on these DFT calculations we assess the solid-solution compounds with respect to their energy density, volume change during intercalation, intercalation voltage and thermal stability. In order to identify trends with average band filling and atomic size we include all combinations of Fe and Mn with elements of the 3d TM series. Moreover, we took into account compounds that verify the observed relations or that are candidate cathode materials, particularly Ni–Co, V–Cu and V–Ni, as well as combinations with 4d TMs (Fe–Zr, Fe–Mo, Fe–Ag) and with Mg (Fe–Mg and Ni–Mg).

This work is organized as follows: in section 2 we present the details of our calculations. The results regarding structural stability are discussed in section 3, followed by an assessment of the electrochemical properties of binary 3d TM compounds in section 4.

2. Computational details

2.1. High-throughput methodology

The systematic screening of binary solid solutions of (Li)$M_yM'_{1-y}PO_4$ is carried out within a high-throughput environment (HTE) for DFT calculations. High-throughput approaches aim to automatize, as far as possible, the vast number of experiments or calculations required for

an extensive screening of compound space. High-throughput screenings with experimental methods can be realized, e.g., by gradients of chemical composition on the same sample [42] as demonstrated recently also for battery materials [43]. High-throughput screenings with numerical calculations based on DFT make use of batch processing and connect to databases or repositories for input and output data. They rely on the transferability of DFT to different chemical elements and have been applied to various material classes (see e.g. [44] for a recent review), including battery materials [45–48]. The benefits of using such an HTE scheme for DFT calculations are (i) the automization of a large portion of routine tasks, (ii) the ability to restart interrupted jobs, (iii) the compatibility with different computing environments and (iv) the organized storage of results for efficient post-processing analysis. The DFT results presented in this work were calculated with an HTE for the VASP code [49–51], similar to previous approaches [47, 52]. It interacts with a repository of structure files on the one hand and the queueing system of the computing environment on the other hand. The HTE loops over the specified lists of structures, exchange-correlation functionals, cutoff energies, k-point densities and initial magnetic moments. For each combination, it generates all input files, submits the job to the queueing system of the computing environment, monitors the status of the calculation and collects the results (e.g. total energy and volume) after completion. Our HTE scheme for DFT calculations has been applied successfully to intermetallics [53, 54] and steels [55–57]; technical details will be described elsewhere [58].

2.2. Ab initio calculations

The self-consistent total-energy calculations presented in the following sections were obtained with DFT using the VASP code [49–51] with projector-augmented wave pseudo-potentials [59]. We used the generalized-gradient approximation [60] to the exchange-correlation functional with effective Hubbard-U parameter. The values of U were taken from Hautier *et al* [61], except for Co [62]. Our convergence tests showed that a plane-wave cutoff of 500 eV and a density of the Monkhorst–Pack $\boldsymbol{k}$-point mesh [63] of 0.020 Å^3 are sufficient to converge the heat of formation to an accuracy of 1 meV/atom. All our calculations included full relaxation of the unit cell and the atoms to residual forces of less than 0.01 eV Å^{-1}.

For all investigated binary solid-solution compounds we assume the olivine-type orthorhombic phosphate crystal structure. This (Li)MPO$_4$ structure with $Pnma$ space group comprises MO$_6$ octahedra and (PO$_4$)$^{3-}$ tetrahedra with strong P–O covalent bonds and a TM cation. In this structure, Li ions can occupy the M1 site and move along the [0 1 0] direction [64] during intercalation. In the following, we occupy the M2 site with metal atoms of one kind or a mixture of two kinds with fraction y in (Li)$M_yM'_{1-y}$PO$_4$. A similar *ab initio* high-throughput screening of such solid solutions on a TM site was also carried out recently for (Li)MM'P$_2$O$_7$, (Li)MM'PO$_4$(OH) and (Li)MM'PO$_4$ [48]. In our study of (Li)$M_yM'_{1-y}$PO$_4$, we use a simulation cell with four M2 sites, which corresponds to steps in TM concentration of 25%. In this simulation cell, we consider two inequivalent atomic arrangements for $y = 0.5$ and one for all other values of y. The two configurations for $y = 0.5$, i.e. for $M : M' = 1 : 1$ compositions, correspond to separation and to intermixing of TM atoms in the M2 sites of [0 0 1] layers. The results presented in the following refer to the arrangement in separate layers that we observed to be energetically favourable. We additionally tested different orderings of the initial atomic moments but found only small differences from the results using ferromagnetic ordering.

We note that this study focuses on replacing Fe and Mn in the olivine-type orthorhombic phosphate in order to understand trends with atomic size and valence-electron number of the substituted element. Even if some of the oxidation states in our calculations are known to

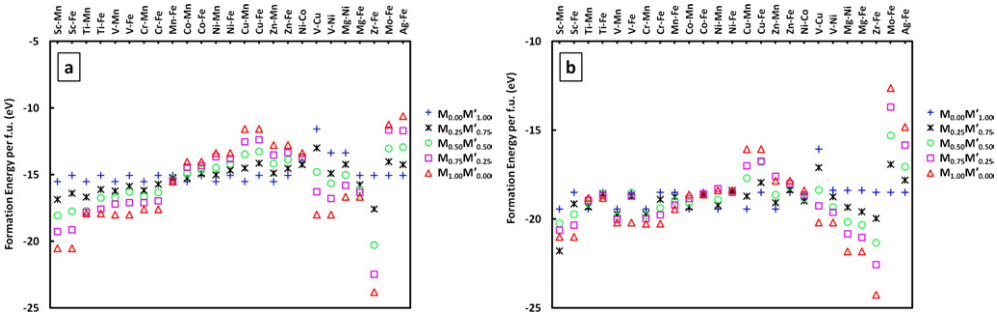

Figure 1. Formation energy of (*a*) non-intercalated and (*b*) intercalated (Li)$M_y M'_{1-y}PO_4$ for composition ranges of $y = 0.0, 0.25, 0.5, 0.75, 1.0$.

be of little thermodynamical significance, they might be kinetically stabilized nevertheless. In particular, in the cases of Sc and Ti, the oxidation state +II is either unknown or very unstable, i.e. pure LiMPO$_4$ would not exist in these cases. Instead, reduction of the de-intercalated compounds MPO$_4$ would lead to reductive cleavage of oxygen, presumably leading to elementary P as the most stable end product. This reaction is aided by formation of covalent bonds in phosphorus and by the greater lattice energies of the resulting oxides. It would be hampered by demixing or by formation of a new phase boundary (unless lattice constants are similar) and volume change. For M = Mg the oxidation state of +III is not known. Its third ionization energy amounts to 80.1 eV, while for 3d TMs, it is roughly between 25 and 35 eV [65]. Zn (39.7 eV) is also an exception, since no Zn(III) compounds are known to exist. In these cases, formation of LiMPO$_4$ is still possible [66] but any attempt at oxidation (deintercalation) would result in oxidation of the covalently bound oxygen atoms instead, resulting in molecular oxygen and solid phosphorus(V) oxide. Therefore, we emphasize that a comprehensive study of the structural stability of competing crystal structures is beyond the scope of this study. For each investigated compound one would need to compute the formation energy of candidate structures in a way demonstrated previously for, e.g., Li–Fe–P–O$_2$ [67] and Li–M–P–O [68]. However, our study identifies trends that may lead to a more refined approach in future work, also with respect to screening electronic properties [69].

3. Structural properties

3.1. Stability

In order to assess the structural stability of the investigated compounds, we computed the formation energy ΔH_f per formula unit (f.u.) from the total energy of the compound E_compound with N_i atoms of constituting element i:

$$\Delta H_\mathrm{f} = E_\mathrm{compound} - \sum_i N_i E_i \tag{1}$$

with respect to the total energies E_i of elements i in their respective ground state. The computed values of the formation energy of the olivine-phosphate structure in different compositions (figure 1) correspond to the stability at zero temperature and zero pressure. We find that all investigated binary compounds have negative formation energy and are hence stable with respect to decomposition into the elements. The stability with respect to other compounds (instead of elements) is not considered here. In order to identify trends, we rather compare

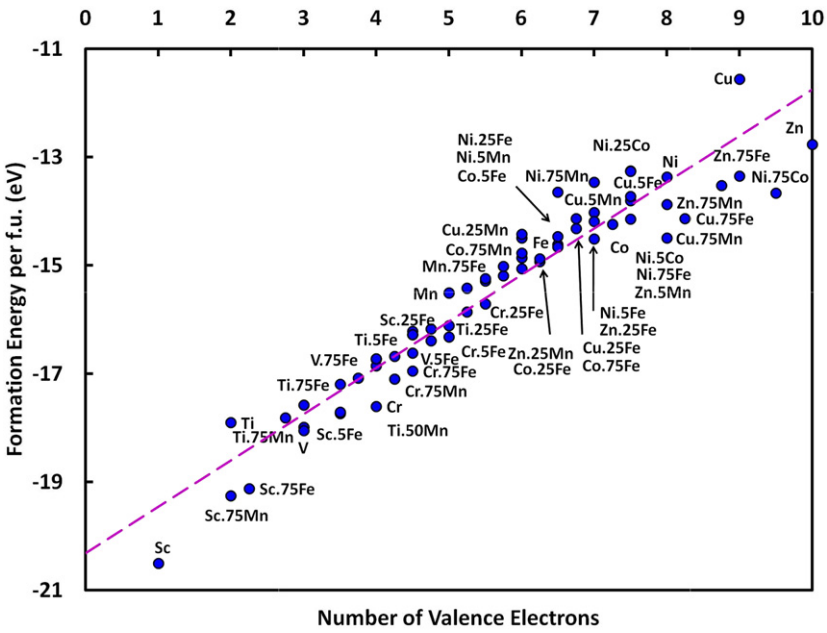

Figure 2. Formation energy of non-intercalated $M_yM'_{1-y}PO_4$ with respect to the average band filling of M and M'. The labels indicate the fraction of M with balance M'.

the compounds with different composition on the same footing, i.e. with the same chemical references.

In most cases, we find an approximately linear variation of the formation energy with variation of the M/M' concentration for both lithiated and non-lithiated olivine phosphate. In order to assess trends of structural stability, we additionally ordered our results compiled in figure 1 with respect to increasing average band filling of the M and M' atoms in figure 2. We identify a fairly linear trend of reduced binding energy for increased average band filling.

The formation energies of the investigated binary solid solutions $(Li)M_yM'_{1-y}PO_4$ can also be related to the formation energies of the compounds with only one type of metal atom in the M2 site, $(Li)MPO_4$ and $(Li)M'PO_4$, by computing the mixing energy

$$\Delta E_{\text{mix}} = E_{(Li)M_yM'_{(1-y)}PO_4} - \left(yE_{(Li)MPO_4} + (1-y)E_{(Li)M'PO_4}\right). \quad (2)$$

The values of $E_{\text{mix}} < 0$ indicate that the formation of a solid solution or ordered $(Li)M_yM'_{1-y}PO_4$ is energetically favourable, whereas $E_{\text{mix}} > 0$ suggests that the system tends to phase-separate into regions of $(Li)MPO_4$ and $(Li)M'PO_4$. The calculated mixing energies for the considered compounds are summarized in figure 3. The variations in the computed mixing energies are up to a few 100 meV. While some compounds, e.g. Co–Mn and Co–Fe, show a tendency of mixing for all investigated $M : M'$ ratios in the lithiated and delithiated stages, other compounds, such as Mo–Fe, show no tendency to form a solid solution at all. For some compounds, e.g. Ti–Fe, the mixing energy turns negative upon delithiation, for other compounds, e.g. Ag–Fe, we observe the opposite behaviour. Therefore, the presence of Li can affect the tendency of M/M' ordering in the M2 site. From a technological point of view we expect those compounds to be more stable to structural rearrangements that exhibit a tendency of mixing at all stages of lithiation. For the case of Fe–Mn, we find an increased mixing

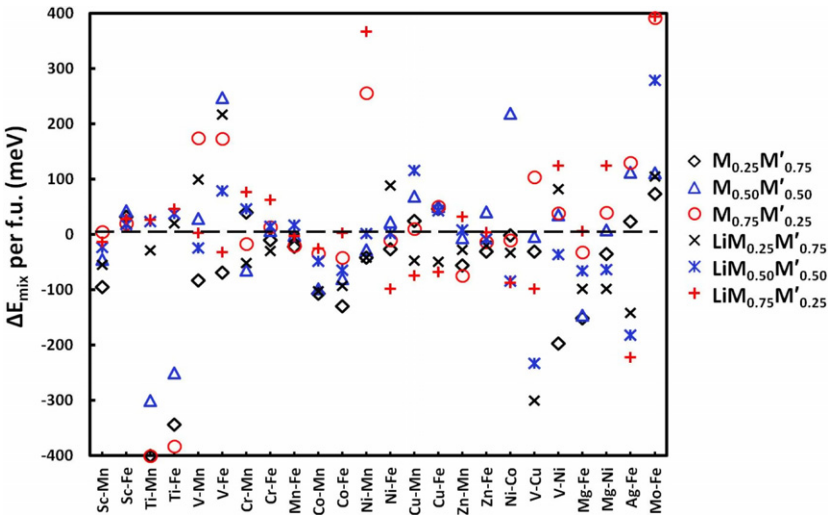

Figure 3. Mixing energy E_{mix} of (Li)$M_yM'_{1-y}PO_4$ for $y = 0.0, 0.25, 0.5, 0.75, 1.0$.

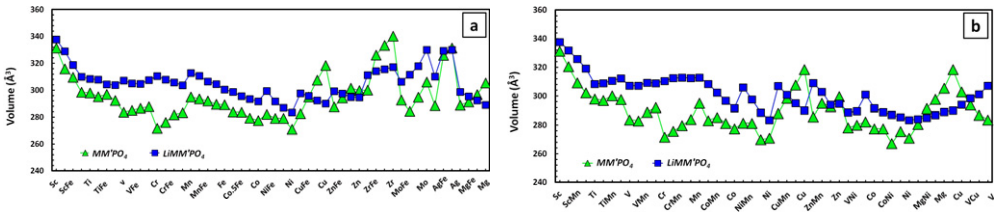

Figure 4. Volume of Li$M_yM'_{1-y}PO_4$ and $M_yM'_{1-y}PO_4$ based on (*a*) Fe and (*b*) Mn or other metals. The labels indicate (Li)MPO_4 and (Li)$M_{0.5}M'_{0.5}PO_4$, respectively, with intermediate compositions in between.

tendency for a larger Fe content, which is consistent with the experimental observation of a mixed phase for Fe-rich compositions only [70].

3.2. Volume change

The Li ions that are inserted into the crystal structure during charging require a certain volume. This may effectively lead to stress on the host lattice and introduce atomic relaxation and a volume change of the crystal structure. The associated elastic energy may give rise to the formation of defects which reduce the long-term cyclability of the Li-ion battery. The degree of deformations due to intercalation depends on the elastic properties of the host crystal. This volume change during intercalation is directly accessible in our DFT calculations by comparing the volume of the fully relaxed simulation cell for the Li$M_yM'_{1-y}PO_4$ and $M_yM'_{1-y}PO_4$ compounds, as shown in figure 4. We observe an overall linear volume decrease of the non-intercalated compound with chemical composition that is in line with experimental observations, e.g., for the substitutions Mn → Fe [40], Fe → Co [40], Mn → Co [40, 71], Fe → Ni [28] and (lithiated) Fe → Mg [16]. In nearly all cases we find a volume expansion due to Li intercalation, e.g. 4.23% for (Li)$FePO_4$ in good agreement with previous *ab initio* calculations [20] (4.2%) and experiments [4] (6.5%). We also confirm the experimental

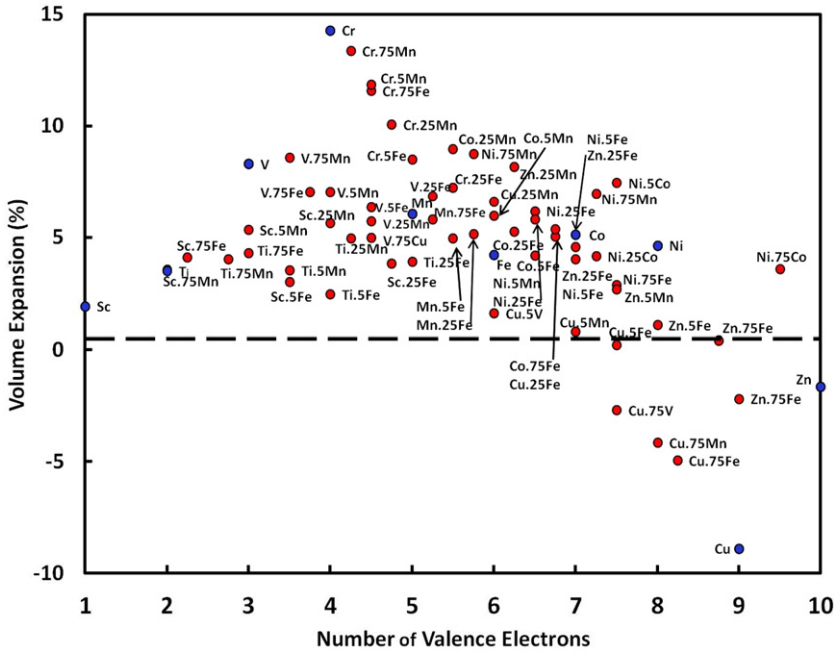

Figure 5. Volume change of (Li)$M_yM'_{1-y}PO_4$ versus average number of valence electrons for 3d TM compounds. Compounds with only one 3d TM are indicated in blue. The labels indicate the fraction of M with balance M'.

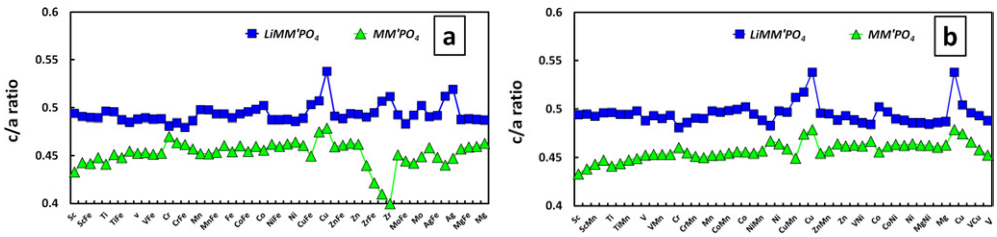

Figure 6. Ratio c/a of Li$M_yM'_{1-y}PO_4$ and $M_yM'_{1-y}PO_4$ based on (a) Fe and (b) Mn or other metals. The labels indicate (Li)MPO_4 and (Li)$M_{0.5}M'_{0.5}PO_4$, respectively, with intermediate compositions in between.

observation that partly replacing Fe with Zn leads to an increased volume of the non-lithiated structure and to a smaller change in volume upon lithiation [32]. The relative volume change as a function of the average number of valence electrons of M and M' is shown in figure 5. Our results indicate that the volume expansion of $LiFePO_4$ can be reduced, e.g., for particular substitution ratios using Sc, Ti, Cu or Zn. We also find that the elements next to Fe in the 3d TM series (V, Cr, Mn, Co and Ni), as well as Ag and Mo tend to increase the volume expansion upon lithiation. Compounds that are rich in Cu, Zn, Zr, Ag and Mg, in contrast, exhibit up to 8.9% volume decrease. The volume decrease with lithiation for Cu was also observed experimentally [31]. Our results for different chemical compositions of the systems Cu–Fe/Mn/V, Zr–Fe and Mg–Ni indicate that this volume decrease can be compensated and turned into a volume increase by substitution.

In addition to the volume we also obtain the values of the c/a ratio of lattice parameters from our structural relaxations that we compiled in figure 6. We find that lithiation increases the

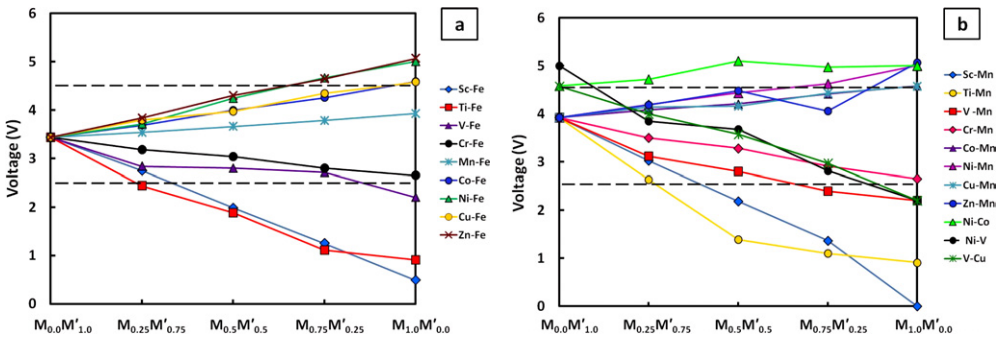

Figure 7. Intercalation voltage of (Li)$M_yM'_{1-y}PO_4$ for 3d TM compounds based on (*a*) Fe and (*b*) Mn or other metals for different M/M' ratios. The dashed lines indicate the technologically relevant voltage regime.

values of the c/a ratio for all investigated compounds. While most compounds show only small variation of the c/a ratio with composition, we find considerable changes for Cu–Fe/Mn/V and Zr–Fe that also showed an increase in volume upon lithiation.

4. Electrochemical assessment of 3d TM binary solid solutions

4.1. Intercalation voltage

In order to identify trends with average band filling we carried out a more detailed assessment of the expected electrochemical properties of the binary 3d TM solid solutions. In particular, we determined the average Li insertion voltage following the approach of Aydinol *et al* [72]. There, the average intercalation voltage between two intercalation limits x_1 and x_2 is given by the difference of their respective Gibbs free energy as

$$\bar{V} = \frac{-\Delta G}{(x_2 - x_1)F} \tag{3}$$

with the Faraday constant F. By approximating ΔG as the difference in internal energy at $T = 0\,\mathrm{K}$, we can directly compute $\bar{V}$ from the difference in the formation energy (figure 1) of the non-intercalated (x_1) and the intercalated (x_2) compound. In the screening approach presented in this work, we are referring to the fully lithiated and the fully delithiated states as the upper limit for the expected intercalation voltage. Capturing the experimentally observed plateaus of electric current during dis-/charge would require much more involved calculations over the full intercalation range (see e.g. [73]) for each considered compound. Our calculated intercalation voltages for the investigated (Li)$M_yM'_{1-y}PO_4$ compounds are summarized in figure 7. We also indicate the technologically relevant voltage regime that requires a sufficiently high energy density (lower limit) within the operating range of the electrolyte (upper limit). In general, we find a linear variation of intercalation voltage with chemical composition (figure 7) that reflects the linear variation of formation energies with composition (figure 1). Considering the $M_{1.0}M'_{0.0}$ compounds with only one TM species, we find an overall increase of the intercalation voltage across the TM series, i.e. with increased band filling. From the 70 investigated compounds, 52 are located in the desirable voltage region of which 28 compounds exhibit an intercalation voltage larger than 3.5 V of $LiFePO_4$. In general, we find that substituting Fe with TM elements to the left of Fe in the periodic table (Sc, Ti, V, Cr, Zr, Mo) reduces the intercalation voltage (except for Mn), while it is increased for TM elements to the right of Fe in the periodic table (Co, Ni, Cu, Zn, Ag). For Mg–Ni and Co–Ni,

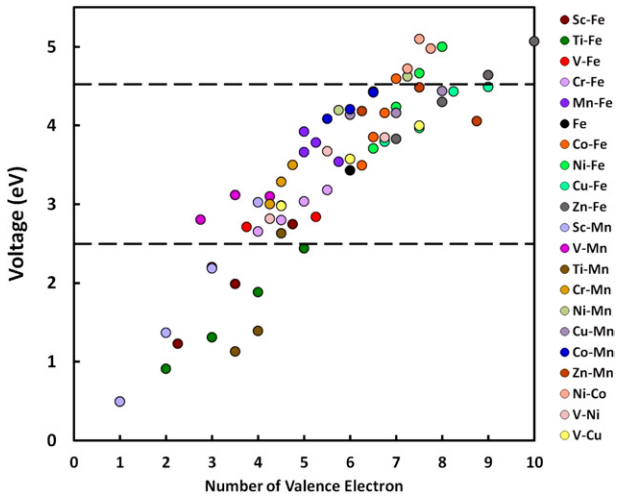

Figure 8. Intercalation voltage of (Li)$M_yM'_{1-y}PO_4$ for 3d TM compounds versus the average number of valence electrons of $M_yM'_{1-y}$. The dashed lines indicate the technologically relevant voltage regime.

the intercalation voltage is above the technologically acceptable limit and seems to be hardly adjustable by the investigated compounds. The compiled variation with chemical composition might help one to identify suitable composition ranges. For example, we find that in several cases the expected intercalation voltage can be increased by decreasing the amount of Fe, in line with previous findings for mixing Fe with Cu [31], Mn [24, 25] or Co [40].

The relation of intercalation voltage (figure 7) and average number of valence electrons of M and M' is shown in figure 8. We observe a fairly linear relation between intercalation voltage and average band filling. This is apparently a consequence of subtracting the linearly varying formation energies (figure 2) in the calculation of the intercalation voltage. Previous DFT calculations [68] allow us to expect that this trend of increased intercalation voltage with increased average band filling also holds for other crystal structures than the olivine phosphates investigated here.

4.2. Gravimetric capacity

The gravimetric capacity measures the maximum charge extractable per unit weight. Here, we assumed that each M/M' atom contributes one electron charge to the capacity and plot the gravimetric capacity for the investigated binary solid solutions of 3d TMs with respect to the intercalation voltage, as shown in figure 9. We find that all compounds based on a combination of two 3d TM atoms show a general trend of reduced gravimetric capacity for increased intercalation voltage. This finding for MM' binary solid solutions is in line with previous DFT calculations [68] for (Li)MPO_4 involving one type of metal atom on the M2 site. Substituting Fe with 4d TM reduces the gravimetric capacity significantly due to the increased weight. Our results also indicate that the specific energy (product of voltage and capacity) is rather low for Sc and Ti substitutions for both Fe- and Mn-based compounds.

4.3. Safety and thermal stability

Meeting the safety demands for commercial battery applications also requires that the cathode material is non-flammable in a wide range of temperatures. Compounds including oxygen

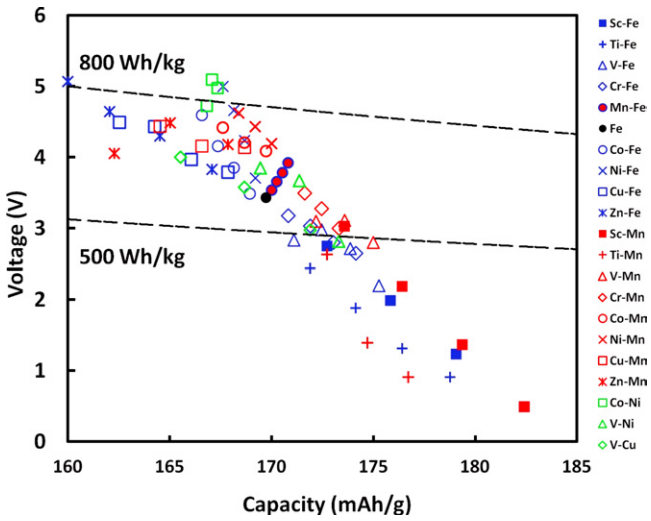

Figure 9. Relation between intercalation voltage and gravimetric capacity of (Li)$M_yM'_{1-y}PO_4$ compounds for 3d TM compounds. The dashed lines indicate selected values of specific energy.

and TMs, such as (Li)$M_yM'_{1-y}PO_4$, can release molecular oxygen in a chain of exothermic processes that, in contact with a flammable electrolyte, may lead to safety problems [74–76]. The relation of thermodynamic oxidation and DFT calculations is given by the oxygen grand potential approximated [67, 76] as

$$\bar{\varphi}(\mu_{O_2}, x_{Li}, x_{Fe}, x_P, \mu_{O_2}) \approx \frac{E - \mu_{O_2} N_{O_2}}{N_{Li} + N_M + N_P} \tag{4}$$

with E the formation energy from DFT, N_i the number of atoms i = Li, M, P per formula unit and μ_{O_2} the oxygen chemical potential at which O_2 is released. Lower values of μ_{O_2} correspond to a more stable cathode at a higher temperature or in a more reducing environment. This methodology has already been applied successfully to high-throughput screening of (Li)–M–P–O phosphates [68] and to tavorite-structured [46] cathode materials. Here we apply this scheme to the 3d TM binary solid-solution compounds under the assumption of the same reaction pathway of oxidation. The identification and energetic investigation of alternative oxidation reactions would require knowledge of the phase diagrams of all investigated Li–M–M'–PO_4 systems. The results of our calculations for the assumed oxidation reaction are shown in figure 10, together with the critical chemical potentials of discharged compounds at which oxygen can be released from a cathode. We find that the critical chemical potential increases with the average number of valence electrons of the MM' solid solution in a fairly linear relation, as indicated in figure 11. This is consistent with previous findings for (Li)MPO_4 [68] involving one type of metal atom on the M2 site and hence demonstrates the viability of our approach to binary solid solutions in olivine phosphates. Regarding the Fe-based compounds, we find that the critical potential μ_{O_2} can be reduced by substituting Fe with earlier TM, i.e. by reducing the average number of d electrons. Replacing Fe with later TM increases μ_{O_2} up to positive values. The same trend holds for substituting Co with either Mn or Ni, and Mn with Co or Ni. In all cases we find that the variation of μ_{O_2} is, to a good approximation, proportional to the fraction of the substitutional material. For the case of Fe–Mn, the increase in the critical μ_{O_2} with increasing Mn content was also observed experimentally in terms of a correspondingly reduced structural stability [70, 71].

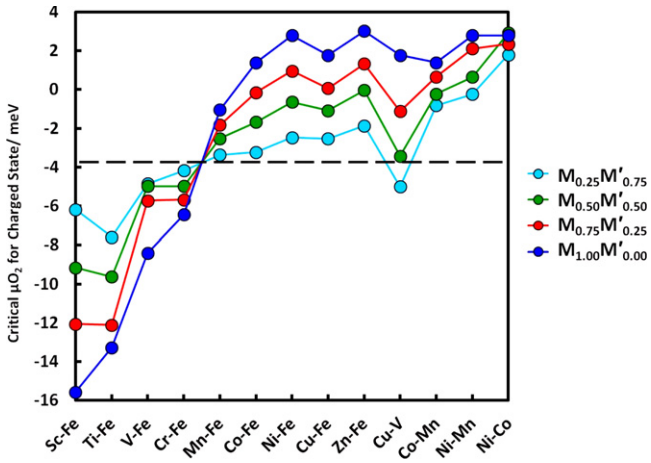

Figure 10. Critical oxygen chemical potential of 3d TM (Li)$M_yM'_{1-y}PO_4$ compounds ordered by increasing average number of valence electrons for $M : M' = 1 : 1$. The dashed line indicates μ_{O_2} for $FePO_4$.

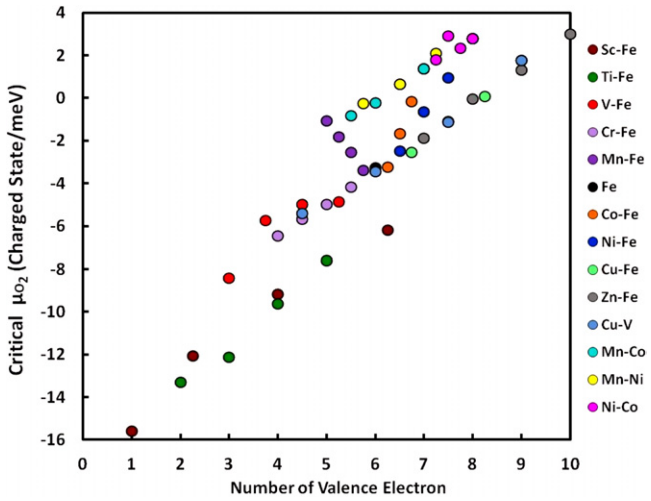

Figure 11. Critical oxygen chemical potential of 3d TM (Li)$M_yM'_{1-y}PO_4$ compounds of figure 10 ordered by increasing average number of valence electrons for all $M : M'$ compositions.

We also computed μ_{O_2} for LiMPO_4 compounds with only one TM and found reasonable agreement with experiments [76–79] and good agreement with previous DFT calculations [76]. For example, for $LiNiPO_4$ and $LiCoPO_4$ we found a positive critical chemical potential and a release temperature of less than approximately 200 °C. This is in good agreement with 100–200 °C for $LiCoPO_4$ [80], and with 150–200 °C for $LiMnPO_4$ [78, 79].

4.4. Volumetric energy density

The volumetric energy density, i.e. the amount of energy stored per unit volume, determines the theoretical capacity for a given battery size. In figure 12 we contrast the volumetric energy density with the critical oxygen chemical potential that is a measure for the thermal

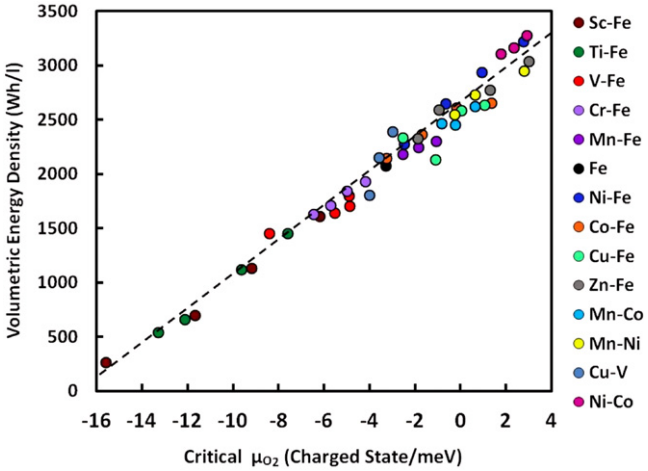

Figure 12. Volumetric energy density as a function of critical oxygen chemical potential for (Li)$M_yM'_{1-y}PO_4$ for 3d TM compounds.

stability. Our calculations suggest that the volumetric energy density is approximately linearly increasing with the critical chemical potential of oxygen for the investigated (Li)$M_yM'_{1-y}PO_4$ compounds. Both quantities tend to increase with average band filling. Hence, the choice of binary solid solution olivine phosphate would correspond to a compromise of reduced thermal stability for increased energy density.

5. Conclusions

With this study we aim to identify general trends and provide hints for future improvements of battery materials. In particular, we carried out a systematic screening by substituting the M2 site in olivine phosphates with binary mixtures of different metal atoms. Using high-throughput density-functional theory calculations we characterized (Li)$M_yM'_{1-y}PO_4$ binary solid solutions according to their formation energy, volume change during intercalation, intercalation voltage, thermal stability and energy density. In order to identify trends with average band filling and atomic size, we include all combinations of Fe and Mn with elements of the 3d TM series, as well as Ni–Co, V–Cu, V–Ni, and combinations with 4d TMs (Fe–Zr, Fe–Mo, Fe–Ag) and with Mg (Fe–Mg and Ni–Mg). We quantify the variation of the (Li)$M_yM'_{1-y}PO_4$ formation energy for $y = 0.0, 0.25, 0.50, 0.75, 1.0$ and in most cases find an approximately linear variation with y for both the intercalated and non-intercalated cases. Our assessment of the tendency to form an ideal solid solution based on the computed mixing energies of all compounds shows a considerable variation with Li concentration. We also observe that replacing Fe with its nearest neighbours in the 3d TM series leads to an increased volume expansion during lithiation. Our assessment of the electrochemical properties of 3d TM binary solid solutions suggests that an increase in average band filling increases the intercalation voltage but reduces the thermal stability. Generally, we find an approximately linear scaling of the investigated properties with $M : M'$ ratio and with average band filling that opens the route to systematically explore the chemical compound space in future studies. The identification of the critical chemical oxygen potential may also give hints for the future synthesis of hitherto unknown compounds which might be stable only under a high oxygen pressure.

Acknowledgments

We acknowledge financial support through the Deutsche Forschungsgemeinschaft within the priority program SPP1473 WeNDeLIB, as well as through ThyssenKrupp AG, Bayer MaterialScience AG, Salzgitter Mannesmann Forschung GmbH, Robert Bosch GmbH, Benteler Stahl/Rohr GmbH, Bayer Technology Services GmbH, the state of North-Rhine Westphalia and the EU in the framework of the ERDF.

References

[1] Fergus J W 2010 Recent developments in cathode materials for lithium ion batteries *J. Power Sources* **195** 939–54
[2] Gong Z and Yang Y 2011 Recent advances in the research of polyanion-type cathode materials for Li-ion batteries *Energy Environ. Sci.* **4** 3223–42
[3] Xu B, Qian D, Wang Z and Meng Y S 2012 Recent progress in cathode materials research for advanced lithium ion batteries *Mater. Sci. Eng.* R **73** 51
[4] Padhi A K, Nanjundaswamy K S and Goodenough J B 1997 Phospho-olivines as positive-electrode materials for rechargeable lithium batteries *J. Electrochem. Soc.* **144** 1188–94
[5] Yamada A, Koizumi H, Nishimura S-i, Sonoyama N, Kanno R, Yonemura M, Nakamura T and Kobayashi Y 2006 Room-temperature miscibility gap in Li_xFePO_4 *Nature Mater.* **5** 357–60
[6] Yamada A, Chung S C and Hinokuma K 2001 Optimized $LiFePO_4$ for lithium battery cathodes *J. Electrochem. Soc.* **148** A224–9
[7] Franger S, Le Cras F, Bourbon C and Rouault H 2003 Comparison between different $LiFePO_4$ synthesis routes and their influence on its physico-chemical properties *J. Power Sources* **119–121** 252–7
[8] Wang Y, Wang J, Yang J and Nuli Y 2006 High-rate $LiFePO_4$ electrode material synthesized by a novel route from $FePO_4{\cdot}4H_2O$ *Adv. Funct. Mater* **16** 2135–40
[9] Ellis B, Kan W H, Makahnouk W R M and Nazar L F 2007 Synthesis of nanocrystals and morphology control of hydrothermally prepared $LiFePO_4$ *J. Mater Chem.* **17** 3248
[10] Ravet N, Chouinard Y, Magnan J F, Besner S, Gauthier M and Armand M 2001 Electroactivity of natural and synthetic triphylite *J. Power Sources* **97–98** 503–7
[11] Yang J and Xu J J 2006 Synthesis and characterization of carbon-coated lithium transition metal phosphates $LiMPO_4$ (M = Fe, Mn, Co, Ni) prepared via a nonaqueous sol–gel route *J. Electrochem. Soc.* **153** A716–23
[12] Gibot P, Casas-Cabanas M, Laffont L, Levasseur S, Carlach P, Hamelet S, Tarascon J-M and Masquelier C 2008 Room-temperature single-phase Li insertion/extraction in nanoscale Li_xFePO_4 *Nature Mater* **7** 741–7
[13] Omenya F, Chernova N A, Zhang R, Fang J, Huang Y, Cohen F, Dobrzynski N, Senanayake S, Xu W and Whittingham M S 2013 Why substitution enhances the reactivity of $LiFePO_4$ *Chem. Mater* **25** 85–9
[14] Chung S-Y, Bloking J T and Chiang Y-M 2002 Electronically conductive phospho-olivines as lithium storage electrodes *Nature Mater* **1** 123–8
[15] Herle P S, Ellis B, Coombs N and Nazar L F 2004 Nano-network electronic conduction in iron and nickel olivine phosphates *Nature Mater* **3** 147–52
[16] Roberts M R, Vitins G and Owen J R 2008 High-throughput studies of $Li_{1-x}Mg_{x/2}FePO_4$ and $LiFe_{1-y}Mg_yPO_4$ and the effect of carbon coating *J. Power Sources* **179** 754–62
[17] Hong J, Wang C S, Chen X, Upreti S and Whittingham M S 2009 Vanadium modified $LiFePO_4$ cathode for Li-ion batteries *Electrochem. Solid-State Lett.* **12** A33–8
[18] Wang G X, Bewlay S, Yao J, Ahn J H, Dou S X and Liu H K 2004 Characterization of $LiM_xFe_{1-x}PO_4$ (M = Mg, Zr, Ti) cathode materials prepared by the sol–gel method *Electrochem. Solid State Lett.* **7** A503–6
[19] Omenya F, Chernova N A, Upreti S, Zavalij P Y, Nam K-W, Yang X-Q and Whittingham M S 2011 Can vanadium be substituted into $LiFePO_4$? *Chem. Mater.* **23** 4733–40
[20] Lin H, Wen Y, Zhang C, Zhang L, Huang Y, Shan B and Chen R 2012 A GGA+U study of lithium diffusion in vanadium doped $LiFePO_4$ *Sol. State Commun.* **152** 999–1003
[21] Yamada A, Takei Y, Koizumi H, Sonoyama N, Kanno R, Itoh K, Yonemura M and Kamiyama T 2006 Electrochemical, magnetic, and structural investigation of the $Li_x(Mn_yFe_{1-y})PO_4$ olivine phases *Chem. Mater* **18** 804–13
[22] Zaghib K, Mauger A, Gendron F, Massot M and Julien C 2008 Insertion properties of $LiFe_{0.5}Mn_{0.5}PO_4$ electrode materials for Li-ion batteries *Ionics* **14** 371–6

[23] Lee K T and Lee K S 2009 Electrochemical properties of $LiFe_{0.9}Mn_{0.1}PO_4/Fe_2P$ cathode material by mechanical alloying *J. Power Sources* **189** 435–9
[24] Kobayashi G, Yamada A, Nishimura S-i, Kanno R, Kobayashi Y, Seki S, Ohno Y and Miyashiro H 2009 Shift of redox potential and kinetics in $Li_x(Mn_yFe_{1-y})PO_4$ *J. Power Sources* **189** 397–401
[25] Malik R, Zhou F and Ceder G 2009 Phase diagram and electrochemical properties of mixed olivines from first-principles calculations *Phys. Rev.* B **79** 214201
[26] Wang D, Ouyang C, Drezena T, Exnar I, Kay A, Kwon N-H, Gouerec P, Miners J H, Wang M and Grätzel M 2010 Improving the electrochemical activity of $LiMnPO_4$ via Mn-site substitution *J. Electrochem. Soc.* **157** A225–9
[27] Wang Z-H, Yuan L-X, Zhang W-X and Huang Y-H 2012 $LiFe_{0.8}Mn_{0.2}PO_4$/C cathode material with high energy density for lithium-ion batteries *J. Alloys Compounds* **532** 25–30
[28] Lee I K, Kim C M, Kim S J and Kim C S 2012 Structural and magnetic phase transition of mixed olivines $Li_xFe_{1-y}Ni_yPO_4$ by lithium deintercalation *J. Appl. Phys.* **111** 07D722
[29] Minakshi M, Sharma N, Ralph D, Appadoo D and Nallathamby K 2011 Synthesis and characterization of $Li(Co_{0.5}Ni_{0.5})PO_4$ cathode for Li-ion aqueous battery applications *Electrochem. Solid State Lett.* **14** A86–9
[30] Minakshi M and Kandhasamy S 2012 Utilizing active multiple dopants (Co and Ni) in olivine $LiMnPO_4$ *Curr. Opin. Solid State Mater Sci.* **16** 163–7
[31] Upreti S *et al* 2011 Crystal structure, physical properties, and electrochemistry of copper substituted $LiFePO_4$ single crystals *Chem. Mater.* **24** 166–73
[32] Liu H, Cao Q, Fu L J, Li C, Wu Y P and Wu H Q 2006 Doping effects of zinc on $LiFePO_4$ cathode material of lithium ion batteries *Electrochem. Commun.* **8** 1553–7
[33] Wang Y, Feng Z-S, Chen J-J, Zhang C, Jin X and Hu J 2012 First principles study on electronic properties and occupancy sites of moybdenum doped into $LiFePO_4$ *Solid State Commun.* **152** 1577
[34] Gwon H, Seo D-H, Kim S-W, Kim J and Kang K 2009 Combined first-principle calculations and experimental study multi-component olivine cathode for lithium rechargeable batteries *Adv. Funct. Mater.* **194** 3285–92
[35] Park Y-U, Kim J, Gwon H, Seo D-H, Kim S-W and Kang K 2010 Synthesis of multicomponent olivine by a novel mixed transition metal oxalate coprecipitation method and electrochemical characterization *Chem. Mater.* **22** 2573–81
[36] Chen Y-C, Chen J-M, Hsu C-H, Lee J-J, Lin T-C, Yeh J-W and Shih H C 2010 Electrochemical and structural studies of $LiCo_{1/3}Mn_{1/3}Fe_{1/3}PO_4$ as a cathode material for lithium ion batteries *J. Power Sources* **195** 6867–72
[37] Kim J, Park Y-U, Seo D-H, Kim J, Kim S-W and Kang K 2011 Mg and Fe co-doped Mn based olivine cathode material for high power capability *J. Electrochem. Soc.* **158** A250–4
[38] Wang X J, Yu X Q, Li H, Yang X Q, McBreen J and Huang X J 2008 Li-storage in $LiFe_{1/4}Mn_{1/4}Co_{1/4}Ni_{1/4}PO_4$ solid solution *Electrochem. Commun.* **10** 1347–50
[39] Seo D H, Gwon H, Kim S-W, Kim J and Kang K 2010 Multicomponent olivine cathode for lithium rechargeable batteries: a first principles study *Chem. Mater.* **22** 518–23
[40] Muraliganth T and Manthiram A 2010 Understanding the shifts in the redox potentials of olivine $LiM_{1-y}M_yPO_4$ (M = Fe, Mn, Co, and Mg) solid solution cathodes *J. Phys. Chem.* C **114** 15530–40
[41] Omenya F, Chernova N A, Zhang R, Fang J, Huang Y, Cohen F, Dobrzynski N, Senanayake S, Xu W and Whittingham M S 2013 Carbon coating of $LiFePO_4$ can be strenghtened by Sc and Ti *J. Phys. Chem.* C **117** 276–9
[42] Ludwig A, Zarnetta R, Hamann S, Savan A and Thienhaus S 2008 Development of multifunctional thin films using high-throughput experimentation methods *Int. J. Mater. Res.* **99** 1144
[43] Borhani-Haghighi S, Kieschnick M, Motemani Y, Savan A, Rogalla D, Becker H-W, Meijer J and Ludwig A 2013 High-throughput compositional and structural evaluation of a $Li_a(Ni_xMn_yCo_z)O_r$ thin film battery materials library *ACS Comb. Sci.* **15** 401
[44] Curtarolo S, Hart G L W, Nardelli M B, Mingo N, Sanvito S and Levy O 2013 The high-throughput highway to computational materials design *Nature Mater.* **12** 192
[45] Ceder G 2010 Opportunities and challenges for first-principles materials design and applications to Li battery materials *Mater. Res. Soc. Bull.* **35** 693
[46] Mueller T, Hautier G, Jain A and Ceder G 2011 Evaluation of tavorite-structured cathode materials for lithium-ion batteries using high-throughput computing *Chem. Mater.* **23** 3854–62
[47] Jain A, Hautier G, Moore C J, Ong S P, Fischer C, Mueller T, Persson K A and Ceder G 2011 A high-throughput infrastructure for density-functional theory calculations *Comput. Mater. Sci.* **50** 2295

[48] Hautier G, Jain A, Mueller T, Moore C, Ong S P and Ceder G 2013 Designing multielectron lithium-ion phosphate cathodes by mixing transition metals *Chem. Mater* **25** 2064–74
[49] Kresse G and Hafner J 1994 *Ab initio* molecular-molecular dynamics simulation of the liquid-metal amorphous–semiconductor transition of germanium *Phys. Rev.* B **49** 14251
[50] Kresse G and Furthmüller J 1996 Efficiency of *ab initio* total energy calculation for metals and semiconductors using a plane-wave basis set *Comput. Mater. Sci.* **6** 15
[51] Kresse G and Furthmüller J 1996 Efficient iterative schemes for *ab initio* total-energy calculations using a plane-wave basis set *Phys. Rev.* B **54** 11169
[52] Curtarolo S, Morgan D and Ceder G 2005 Accuracy of *ab initio* methods in predicting the crystal structures of metals: a review of 80 binary alloys *CALPHAD* **29** 163
[53] Hammerschmidt T, Seiser B, Drautz R and Pettifor D G 2008 Modelling topologically close-packed phases in superalloys: valence-dependent bond-order potentials based on *ab initio* calculations *Superalloys 2008* ed R C Reed *et al* (Warrendale, PA: The Metals, Minerals and Materials Society) p 847
[54] Seiser B, Hammerschmidt T, Kolmogorov A N, Drautz R and Pettifor D G 2011 Theory of structural trends within 4d and 5d transition metals topologically close-packed phases *Phys. Rev.* B **83** 224116
[55] Kolmogorov A N, Shah S, Margine E R, Bialon A F, Hammerschmidt T and Drautz R 2010 New superconduting and semiconducting Fe–B compounds predicted with an *ab initio* evolutionary search *Phys. Rev. Lett.* **105** 217003
[56] Bialon A F, Hammerschmidt T, Drautz R, Shah S, Margine E R and Kolmogorov A N 2011 Possible routes for synthesis of new boron-rich Fe–B and $Fe_{1-x}Cr_xB_4$ compounds *Appl. Phys. Lett.* **98** 081901
[57] Bialon A F, Hammerschmidt T and Drautz R 2013 *Ab initio* study of boron in α-iron: migration barriers and interaction with point defects *Phys. Rev.* B **87** 104109
[58] Hammerschmidt T, Bialon A F, Pettifor D G and Drautz R 2013 *New J. Phys.* submitted
[59] Blöchl P 1994 *Phys. Rev.* B **50** 17953
[60] Perdew J P, Burke K and Ernzerhof M 1996 Generalized gradient approximation made simple *Phys. Rev. Lett.* **77** 3865
[61] Hautier G, Ong S P, Jain A, Moore C J and Ceder G 2012 Accuracy of density functional theory in predicting formation energies of ternary oxides from binary oxides and its implication on phase stability *Phys. Rev.* B **85** 155208
[62] Zhou F, Cococcioni M, Kang K and Ceder G 2004 The Li intercalation potential of $LiMPO_4$ and $LiMSiO_4$ olivines with M = Fe, Mn, Co, Ni *Electrochem. Commun.* **6** 1144–8
[63] Monkhorst H J and Pack J D 1976 Special points for Brillouin-zone integrations *Phys. Rev.* B **13** 5188
[64] Dathar G K P, Sheppard D, Stevenson K J and Henkelman G 2011 Calculations of Li-ion diffusion in olivine phosphates *Chem. Mater.* **23** 4032–7
[65] Binder H H 1999 *Lexikon der Chemischen Elemente* (Leipzig: Hirzel)
[66] El Ammari L and Elouadi B 1989 Structure of alpha-$LiZnPO_4$ *Acta Crystallogr.* C **45** 1864
[67] Ong S P, Wang L, Kang B and Ceder G 2008 Li–Fe–P–O_2 phase diagram from first principles calculations *Chem. Mater.* **20** 1798–807
[68] Hautier G, Jain A, Ong S P, Kang B, Moore C, Doe R and Ceder G 2011 Phosphates as lithium-ion battery cathodes: an evaluation based on high-throughput *ab initio* calculations *Chem. Mater.* **23** 3495–508
[69] Zhou F, Kang K, Maxisch T, Ceder G and Morgan D 2004 The electronic structure and band gap of $LiFePO_4$ and $LiMnPO_4$ *Solid State Commun.* **132** 181–6
[70] Kim J, Park K-Y, Park I, Yoo J-K, Hong J and Kang K 2012 Thermal stability of Fe–Mn binary olivine cathodes for Li rechargeable batteries *J. Mater. Chem.* **22** 11964–70
[71] Nolis G M, Omenya F, Zhang R, Fang B, Upreti S, Chernova N A, Wang F, Graetz J, Hu Y-Y, Grey C P and Whittingham M S 2012 Structure, defects and thermal stability of delithiated olivine phosphates *J. Mater. Chem.* **22** 20482–9
[72] Aydinol M K, Kohan A F, Ceder G, Cho K and Joannopoulos J 1997 *Ab initio* study of lithium intercalation in metal oxides and metal dichalcogenides *Phys. Rev.* B **56** 1354
[73] Breger J, Meng Y S, Hinuma Y, Kumar S, Kang K, Shao-Horn Y, Ceder G and Grey C P 2006 Effect of high voltage on the structure and electrochemistry of $LiNi_{0.5}Mn_{0.5}O_2$: a joint experimental and theoretical study *Chem. Mater.* **18** 4768–81
[74] Liu Y, Mi C, Yuan C and Zhang X 2009 Improvement of electrochemical and thermal stability of LiFePO4 cathode modified by CeO_2 *J. Electroanal. Chem.* **628** 73–80
[75] Xu K 2004 Nonaqueous liquid electrolytes for lithium-based rechargeable batteries *Chem. Rev.* **104** 4303–418
[76] Ong S P, Jain A, Hautier G, Kang B and Ceder G 2010 Thermal stabilities of delithiated olivine MPO_4 (M = Fe, Mn) cathodes investigated using first principles calculations *Electrochem. Commun.* **12** 427–30

[77] Delacourt C, Poizot P, Tarascon J-M and Masquelier C 2005 The existence of a temperature-driven solid solution in Li_xFePO_4 for $0 \leqslant x \leqslant 1$ *Nature Mater.* **4** 254–60

[78] Kim S-W, Kim J, Gwon H and Kang K 2009 Phase stability study of $Li_{1-x}MnPO_4$ ($0 \leqslant x \leqslant 1$) cathode for Li rechargeable battery *J. Electrochem. Soc.* **156** A635–8

[79] Chen G and Richardson T J 2010 Thermal instability of olivine-type $LiMnPO_4$ cathodes *J. Power Sources* **195** 1221–4

[80] Bramnik N N, Nikolowski K, Trots D M and Ehrenberg H 2008 Thermal stability of $LiCoPO_4$ cathodes *Electrochem. Solid State Lett.* **11** A89–93